

Optimization of Asteroid Capture Missions using Earth Resonant Encounters

Rita Neves and Dr. Joan Pau Sánchez

Abstract This paper describes a robust methodology to design Earth-resonant asteroid capture trajectories leading to Libration Point Orbits (LPOs). These trajectories consider two impulsive manoeuvres; one occurring before the first Earth encounter and a final one that inserts the asteroid into a stable hyperbolic manifold trajectory leading to an LPO of the Sun-Earth system. The first manoeuvre is key to exploit the chaotic perturbative effects of the Earth and obtain important reductions on the cost of inserting the asteroid into a manifold trajectory. The perturbative effects caused by the Earth are here modelled by means of a Keplerian Map approximation, and these are posteriorly compared with the dynamics of the Circular Restricted Three-Body Problem. Savings in the order of 50% of total Δv are computed for four different asteroids.

Key words: Asteroid Capture; Earth-Resonant Encounters; Trajectory Optimization; Libration Point Orbits

1 Introduction

Asteroid capture and retrieval missions have been getting the attention of the scientific community for some years. There are thousands of asteroids in orbits relatively close to the Earth and new ones are discovered often; as of January 2017, there are over 15 000 observed near-Earth asteroids (NEA), from which 5% were only reported the year before.⁵ The characteristics of most NEA are still unknown,

Rita Neves
Cranfield University, College Road, Cranfield MK43 0AL, UK
e-mail: r.neves@cranfield.ac.uk

Dr. Joan Pau Sánchez
Cranfield University, College Road, Cranfield MK43 0AL, UK
e-mail: j.p.sanchez@cranfield.ac.uk

from size to material composition. As such, these bodies are considered very interesting targets for investigation. From data collection, to technology demonstrations or in-situ resource utilization, there are many scientific operations that can be undertaken, which presents an opportunity for challenging mission scenarios.

Asteroid capture missions are characterized by the rendezvous of a spacecraft with an asteroid and moving it to an orbit in the vicinity of the Earth. The spacecraft is utilised to modify the celestial body's trajectory in such a way as to make it enter the target orbit; the utilization of Solar Electric Propulsion (SEP) is one possible technology for this endeavour,⁹ although some others have been studied.

This work proposes to minimise the total fuel consumption, here regarded as Δv_C , of capturing an asteroid into a Libration Point Orbit (LPO). For this objective to be achieved, a manoeuvre that takes the asteroid from its nominal orbit to the destination has to be performed. This is the case studied by Yáñez et al.,¹¹ which considers a single Δv change that alters the asteroid's orbit to the one of the invariant manifold leading to the LPO, creating a database for Easily Retrievable Asteroids (EROs) by noting the capture Δv of several bodies.

This work intends to exploit the chaotic nature of our Solar System and its numerous gravitational perturbations to find low-energy trajectories that lead to the capture of NEA into LPO. In this way, a different approach is proposed: the application of an initial manoeuvre Δv_M for an optimal passage near the Earth, which is thereafter referred as an *Earth-resonant encounter*, and the final Δv_I insertion into the LPO. It is proposed that the initial manoeuvre Δv_M can be optimized in such a way that the resonant encounter with the Earth impacts the asteroid's orbital elements optimally, so that the total cost of the trajectory is lower than for a direct capture.

In order to model an asteroid's motion, the Keplerian Map (KM) equations are used. This is a perturbative model that allows for the simulation of Earth's gravitational influence on the body's orbit around the Sun, while being less computationally expensive than higher fidelity models such as the Circular Restricted Three-Body Problem (CR3BP). Given that the number of asteroids to be considered for capture is very high, utilizing this model is a way to decrease computational time. This is essential in space mission design, where several variables may have to be taken into account and, thus, extensive search spaces must be explored.

The present paper is organized as follows. Section 2 makes an overview on manifold theory and LPO, as well as detailing the dynamical models used for the presented asteroid capture trajectories, namely the KM. Section 3 analyses the full trajectory design and explains the procedure to obtain the best solution and its refinement with a higher order model. Section 4 reports the results for four different asteroids, studying the savings in Δv_C and the impact on the capture's time of flight. Finally, Section 5 evaluates the implications of these developments and highlights some points that may benefit from further work.

2 Near-Earth Asteroids

NEA have been so far classified according to their orbits and divided into four main categories: Amors, Apollos, Atens and Atiras. Amor asteroids stay always outside Earth's orbit and never cross it; Apollos and Atens cross Earth's orbit, but the former still have a wider orbit than the planet, while the latter are characterized for staying longer inside Earth's orbit and having smaller semi-major axes; Atiras remain confined inside Earth's orbit throughout their motion. These categories are depicted in Figure 1.

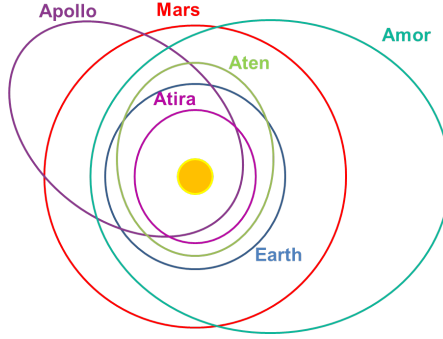


Fig. 1: Orbits of different NEA categories in the Solar System

The purpose of this work is to develop low-energy trajectories, using Earth-resonant encounters, that lead a NEA to an LPO. The latter are not the only near-Earth orbits that can be used for asteroid capture, but the asteroid population that can be cheaply moved into such an orbit may not be the same as into others (such as Distant Retrograde Orbits or DRO), as reported by Sánchez & Yárnoz,⁸ making these interesting targets for investigation.

2.1 LPO and Invariant Manifolds

The Libration or Lagrangian points are positions in space where an object of negligible mass, affected by the gravitational interactions between two larger bodies (the primary and the secondary), can maintain a stationary position. These points are generally represented in a synodic reference frame, in which the primaries appear to be static while the third body rotates around them. They are very attractive for a great number of missions, namely to hold telescopes or other observation-type spacecraft, since the fuel consumption required to perform station-keeping is very low.

Several types of periodic orbits can be found around these points, from which we highlight three: Horizontal Lyapunov orbits, which are in the ecliptic plane, Vertical Lyapunov orbits, that are horizontally symmetric and shaped like a figure-eight, and Halo orbits, which bifurcate from the Horizontal Lyapunov orbit family; these can be seen on Figure 2. An infinite number of quasi-periodic orbits can also be found, divided into two families: Lissajous around the Vertical Lyapunov orbits, and the Quasi-Halos around the Halo orbits.¹

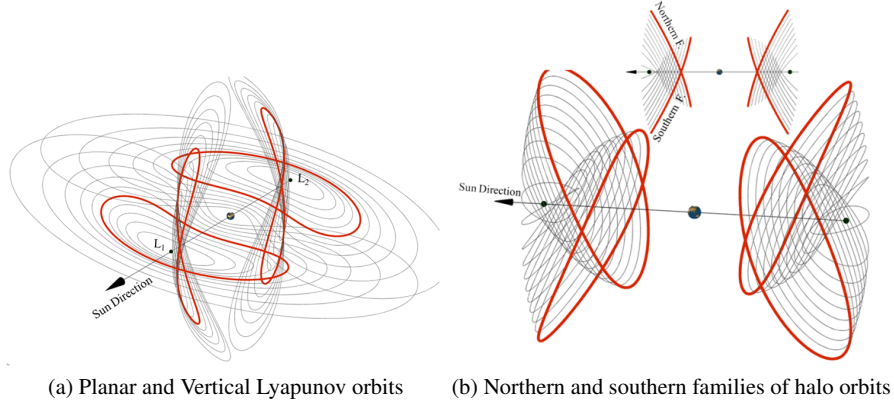


Fig. 2: Libration Point Orbits associated with the Sun-Earth L_1 and L_2 points⁸

Hyperbolic invariant manifolds, dynamical structures composed of countless orbits, are connected to the LPOs.² Mathematically, these are defined as sets of points in the system's phase space that tend toward a given limit as time tends to plus or minus infinity; they exist for a range of energies and form a series of 'tubes' connecting different regions around the primaries. These invariant manifold tubes can be used to explore new spacecraft trajectories with interesting characteristics: by moving one body to an invariant manifold orbit connected to an LPO, it will arrive there without any further manoeuvring.

2.2 The Keplerian Map

Considering that the asteroid encounters the Earth at some point along its trajectory, it is necessary to take into account its perturbative influence on the mission design. Since the considered asteroids move outside Hill sphere, it is infeasible to use a patched-conics method; therefore, we resort to the KM, a perturbation model for the motion of an object orbiting a central body.

The KM influence is factored in using a first-order approximation of Picard's iteration on Lagrange's planetary equations. Its equations can be used to calculate the changes in orbital elements caused by the perturbing object, which are computed at each periapsis passage of the body, and then added to the previously known orbital elements.⁴ In this way, the action of the KM can be represented by the mapping \mathcal{H} :

$$\mathcal{H} : \{a, e, i, \omega | \alpha\} \mapsto \{\Delta a, \Delta e, \Delta i, \Delta \omega | \alpha\} \quad (1)$$

The parameter α accounts for the phasing of the perturbed body with the one provoking the disturbance: in a synodic reference frame with the Sun (central body) and the Earth (perturbing body) as primaries, it is the angle in between the Sun-Earth line and the projection of the Sun-asteroid line in the ecliptic plane. Since the KM is only computed at α values in which a periapsis passage occurs, these are uniquely named α_P . Considering the asteroid's movement, the value of $\Delta \alpha_P$ has also to be updated to represent the following periapsis passage, using this equation:

$$\alpha_{P_{n+1}} = \alpha_{P_n} + 2\pi \left| \sqrt{\frac{a_{n+1}^3}{1-\mu}} - 1 \right| \quad (2)$$

in which n indicates in which time step the computation is being made, a represents the asteroid's semi-major axis and μ is the normalized gravitational parameter of the system.

On Figure 3, we can observe the movement of asteroid 2016RD34 in the synodic reference frame; polar axes were juxtaposed to these, showing the range of α . One of the periapsis passages happening during the Earth-resonant encounter is highlighted, revealing $\alpha_P = 4.3^\circ$.

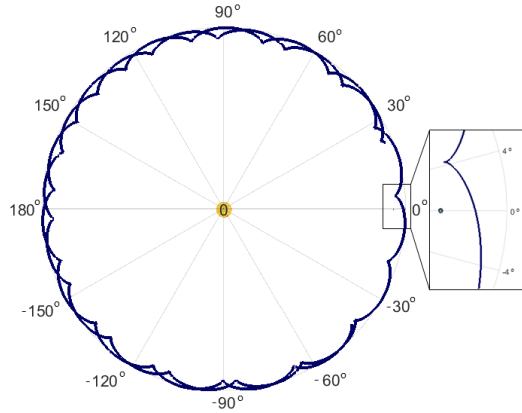


Fig. 3: Phasing α_P for an Earth-resonant encounter for asteroid 2016RD34

An interesting application of the KM is the kick-map, a visual representation of the orbital elements changes as a function of the object's phasing with the perturbing body. As an example, Figure 4 shows the semi-major axis change undergone by asteroid 2016RD34 depending on the angle α_P ; this is, then, the kick-map that matches the movement shown in Figure 3. In this way, the value of Δa corresponding to $\alpha_P = 4.3^\circ$ can be simply taken from this plot—on Figure 4, it is represented by the crossing of dotted lines.

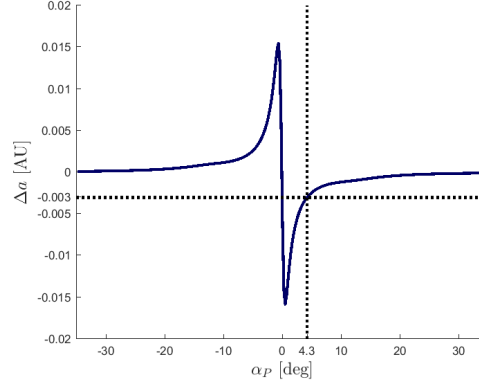


Fig. 4: Kick-map: change in Δa with α for a resonant encounter of asteroid 2016RD34

The study of the kick-map also allows for the assertion that, for specific values of α_P , the orbital element change can be quite significant, while for others the perturbing body's influence is barely felt.

3 Trajectory Design

The proposed trajectory consists on manoeuvring the asteroid for an optimal resonant encounter with the Earth and posterior capture into an LPO. Therefore, it can be divided into three distinct sections, highlighted in Figure 5. The first section, Phase A, starts when the asteroid is at the periapsis, right outside the perturbative region of influence of the Earth; at this point, the asteroid's velocity is changed by Δv_M , altering its path. The second section, Phase B, corresponds to the resonant encounter with the Earth, in which the asteroid is affected by its perturbation. This region was defined by $|\alpha| = \frac{\pi}{8} + \frac{\Delta\alpha}{2}$, which delimits a sufficiently large zone to encompass all α_P in which the object's motion is noticeably perturbed. The third section, Phase C, ends at the insertion of the asteroid into an invariant manifold connected to an LPO

by performing a manoeuvre of cost Δv_I . The final capture Δv_C is the added total of the two different manoeuvres, Δv_M and Δv_I .

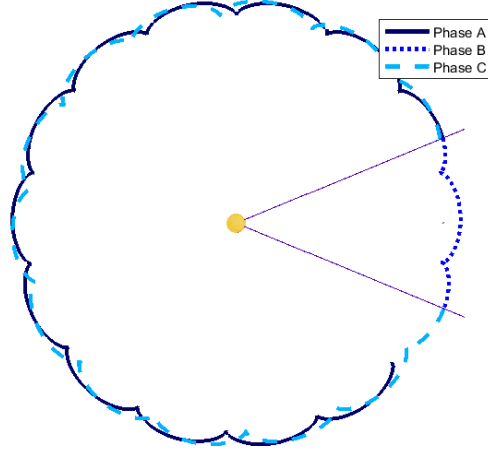


Fig. 5: Phases of the capture trajectory with an Earth-resonant encounter

The asteroid's motion during Phases A and C is Keplerian around the Sun; its path is only altered by Δv_M on the former case. However, due to the close proximity with the Earth, Phase B has the object in a three-body configuration, where its movement is modelled with the KM. One simplification must be mentioned: although Δv_M will cause a change in the orbital elements before the Earth-resonant encounter, it is so small that makes no difference in the application of the KM model. In this way, the mapping shown on Equation 1 was performed with the original set of orbital parameters, regardless of the application of Δv_M .

3.0.1 Initial Filtering

In order to assess which asteroids show reductions in capture cost by the implementation of this trajectory, a list of all discovered NEA orbital elements was collected from the Minor Planet Center's database. Considering over 15000 candidates, pruning had to be performed for this study to be feasible.

For this purpose, a filter that computes an estimate of the insertion cost Δv_I in the LPO, based on a direct capture using a bi-impulsive manoeuvre, was designed. This was first described by Sánchez et. al⁶ and later expanded.⁸ It has proved to be a good lower threshold of the real capture manoeuvre and, as such, is used in the

current paper to estimate Δv_I for the computed trajectories. For completeness, this section includes a brief summary of how the filter works.

The bi-impulsive manoeuvre considers one burn on the perihelion and one on the aphelion, in which only one of the two is responsible for an inclination correction, and both include a semi-major axis change. This is described by Equation 3:

$$\Delta v_I = \sqrt{\Delta v_{a1}^2 + \Delta v_{i1}^2} + \sqrt{\Delta v_{a2}^2 + \Delta v_{i2}^2} \quad (3)$$

in which Δv_a is the classical change in semi-major axis manoeuvre, whereas Δv_i is the inclination change.

Thus, there are four computed values for Δv_I , depending on whether the perihelion or aphelion burn is the first and which of them will include the inclination correction; the lowest value out of these will be the filter output.

The filter application allowed, using an established ceiling of 1.2 km/s, to restrict our search to 61 asteroids. Posteriorly, the ephemerides from this reduced list were taken from the Horizons JPL database;³ the time period for data collection was from 2020 to 2100. One synodic period, out of all comprised in this time span, was chosen: the one with highest optimization sensitivity, corresponding to the one where the orbital elements suffer the greatest change as caused by the Earth.

3.0.2 Grid Search

In Figure 6, we observe the application of Δv_M changes the asteroid's movement and encounter with the Earth, as opposed to its original path. It is important to denote that, for all the figures in this paper, the Earth is not in scale, but was plotted instead with the radius of Hill sphere. We can discern how a small change of the asteroids' orbital elements leads to a different encounter; therefore, our purpose is to develop a trajectory that leads to the cheapest capture possible by exploiting this effect. In order to achieve this, a grid search was performed for the Δv_M corresponding to the lowest Δv_C .

As mentioned in Section 3, the KM is computed only for the initial asteroid's elements; as such, the orbital element changes will repeat themselves after the asteroid's orbit is moved forwards or backwards one epicycle, since α_P values will be the same. Thus, the analysis is restricted to Δv_M inside limits that correspond to the asteroid moving backwards or forwards one epicycle. These are easily computed resorting to Gauss' form of the variational equations,⁶ as following:

$$\Delta v_M = \frac{\mu_{Sun} \Delta a}{2a^2 v_P} \quad (4)$$

where μ_{Sun} is the Sun's gravitational constant, v_P is the velocity at the periapsis and Δa represents the variation in initial semi-major axis corresponding to the addition of an extra epicycle to the asteroid's motion. The latter is computed using the equations:

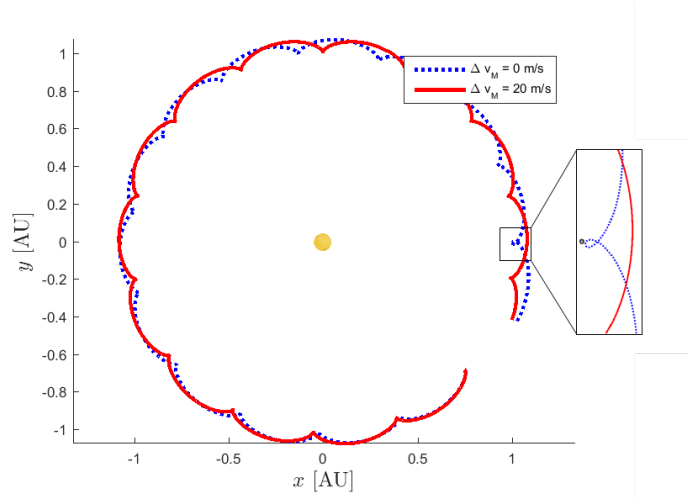


Fig. 6: Comparison of asteroid 2016RD34 trajectory with different initial values of Δv_M

$$\Delta a = \frac{\sqrt{1-\mu}\Delta\alpha}{3\pi n_P \sqrt{a}} \quad (5)$$

where μ is the normalized gravitational constant of the system, n_P is the number of periapsis passages occurring from the manoeuvre to the target point and $\Delta\alpha$ is the angular span of one epicycle:

$$\Delta\alpha = 2\pi \left(\sqrt{\frac{a^3}{1-\mu}} - 1 \right) \quad (6)$$

Once the limits are obtained, all the values of Δv_C are computed for Δv_M inside the established limits, with a step change of 0.2 m/s.

3.0.3 Refinement

After obtaining a solution using the method detailed in Subsection 3.0.2, the trajectory was refined with a higher fidelity model: namely, the CR3BP. This dynamical model is very well established for orbital motion, having been used countless times in mission analysis.¹⁰

For the purpose of obtaining a more refined solution, the CR3BP simulation has to be matched with the KM motion. Due to the higher sensitivity of the former, this may not be achieved by propagating the asteroid's motion using the orbital elements obtained after the Δv_M manoeuvre.

In general terms, the closer the asteroid is to the perturbing body, the greater its influence on it; as such, the object may undergo several periapsis passages in the region of the Earth's perturbation, but the one that will exert the most significant impact on its motion will be the one in which α_P is the closest to zero. Following this logic, in order to get a similar orbital change for the CR3BP as from the KM, the closest of its periapsis passages, $\alpha_{closest}$, should be the same as in the KM.

In order to target $\alpha_{closest}$, we employ a bisection method: this is implemented by defining upper and lower bounds to a trial Δv_M and propagating the motion in the CR3BP using their mean value. Depending on whether the asteroid has surpassed or fallen behind $\alpha_{closest}$, the limits to the manoeuvre are changed and the consequent trial Δv_M is altered accordingly.

On Figure 7, we can observe the evolution of the semi-major axis throughout time, for the entire trajectory, as depicted in Figure 5. Three plots can be distinguished: the propagation using the KM with the grid search solution ($\Delta v_M = -7.4$ m/s), with the CR3BP using the same manoeuvre and, finally, using the Δv_M provided by the targeting method ($\Delta v_M = -6.6$ m/s). The latter option matches the first one much more accurately, reinforcing the choice to apply the targeting procedure.

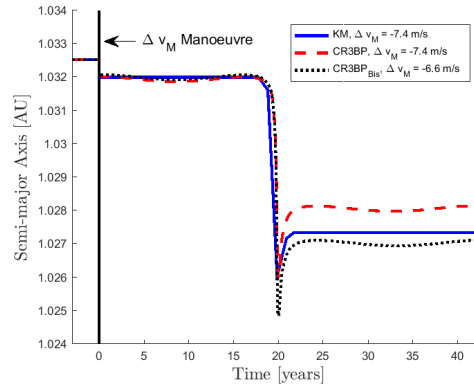


Fig. 7: Evolution of the semi-major axis of asteroid 2011BL45 throughout time

4 Results and Discussion

From the list of 61 asteroids that were filtered with a threshold of $\Delta v_f = 1.2$ km/s, the ones presented in this paper are the four that benefit the most from the Earth-resonant encounter trajectory. In order to find these, three capture scenarios were compared and shown in Figure 8. Case 1 considers the cost of capturing an asteroid without any resonant encounter with the Earth; Case 2 examines a capture after the Earth-resonant encounter, but with no interference on the asteroid's

path. Both these cases are used as benchmarks for comparison with our studied trajectory—the resonant capture with optimal manoeuvring Δv_M , depicted by Case 3.

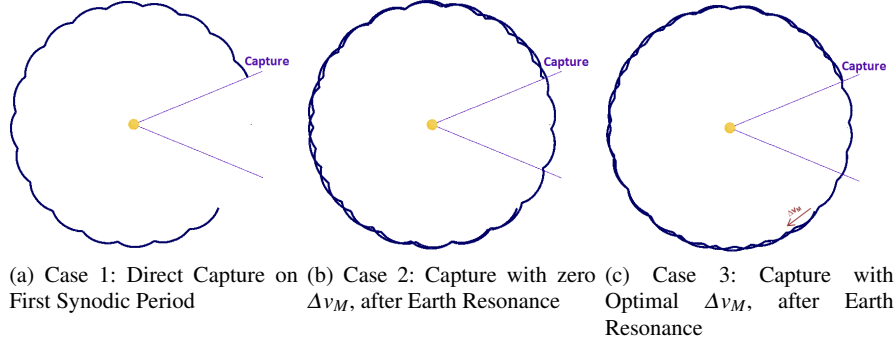


Fig. 8: Capture Cases for asteroid 2011BL45

The asteroids selected were the ones presenting the highest savings in fuel consumption as compared to Cases 1 and 2. These results are presented on Table 1:

Table 1: Asteroid capture costs for each Case, in [m/s]

Asteroid	Δv_M	Δv_{Case1}	Δv_{Case2}	Δv_{Case3}	Δv_{CR3BP}	Fuel Reduction
2011BL45	-7.4	88.0	116.1	48.4	45.1	45.0% ¹
2010VQ98	-2.6	255.3	470.4	112.2	120.1	56.1% ¹
2008UA202	-13.6	307.3	307.6	189.0	214.5	38.5% ¹
2016RD34	-2.8	317.6	508.0	125.3	281.2	60.6% ¹

¹ Compared to Case 1

² Compared to Case 2

Two fuel reduction computations were obtained from comparing Case 3 to Cases 1 and 2; the value shown in Table 1 is the lowest of them, in order to highlight the asteroids in which Case 3 is clearly the most cost efficient. There are, however, asteroids which benefit greatly from a resonant trajectory, but in which the manoeuvre is not essential (i.e. asteroid 2011MD), which means that the Δv of Cases 2 and 3 is similar—these were, consequently, left out of this discussion.

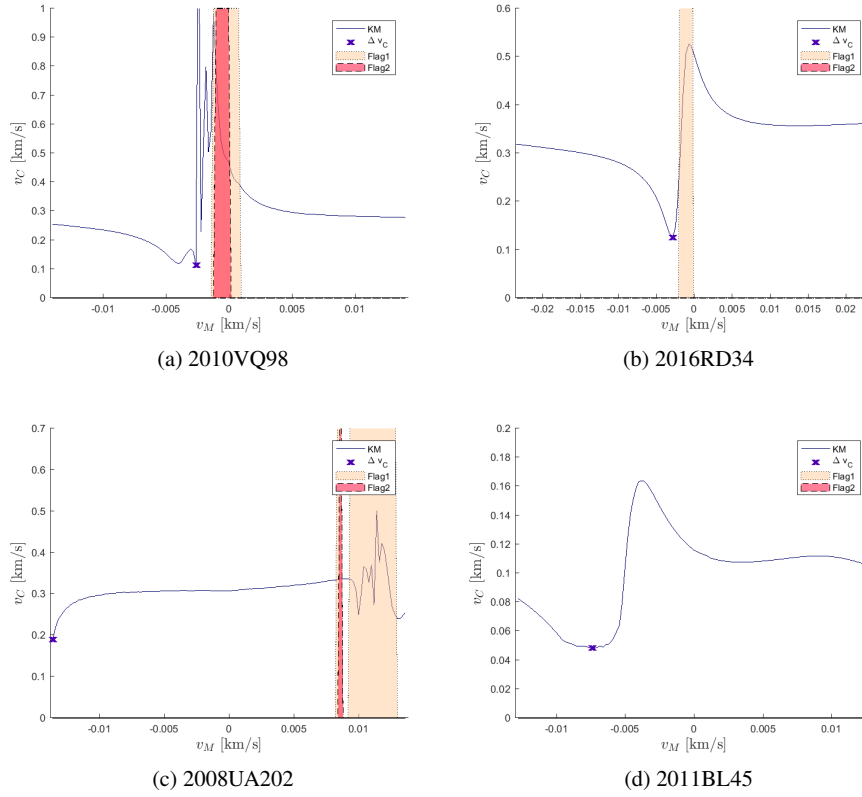
From Table 1, we observe that the obtained fuel reduction is very high, ranging from 38.5% to 60.6%. The Δv obtained for Cases 1 and 2 are very different; they correspond, in fact, to capture on two distinct synodic periods where substantial perturbation by the Earth was occurring regardless of any manoeuvre. However, in

Table 2: Asteroid data and times of flight for capture manoeuvre, in years

Asteroid	NEA Category	Capture LPO	Starting Date	TOF_{Case1}	TOF_{Case3}
2011BL45	Amor	VL_2^1	19/08/2073	17.6	42.4
2010VQ98	Apollo	VL_2^1	10/11/2063	16.6	46.3
2008UA202	Apollo	PL_2^2	29/02/2020	29.4	41.3
2016RD34	Amor	VL_2^1	18/10/2033	12.9	35.4

¹ Vertical Lyapunov in L_2 ² Planar Lyapunov in L_2

the depicted cases, a very small Δv_M corresponded to a significant decrease in Δv_C for Case 3, as can be observed in Figure 9.

Fig. 9: Asteroid capture Δv_C as a function of the initial manoeuvring Δv_M

In these figures, we can distinguish two coloured areas, *Flag1* and *Flag2*. *Flag1* is raised when the asteroid is moving inside the Hill sphere, whereas *Flag2* appears when the perturbation is so strong that a transition occurs, meaning the asteroid's semi-major axis decreases from greater to smaller than one, or vice-versa; in both these cases, the KM should not be used to compute the body's motion, as previously mentioned in Section 2.2. It is possible to see how chaotic the plot behaviour becomes in these areas, corroborating this decision.

The refinement of Δv_{Case3} values with the CR3BP is shown on Table 1, represented by the parameter Δv_{CR3BP} . The targeting of $\alpha_{closest}$ using the bisection method converges quickly with great results: the error for the targeted angle reduces to less than 10^{-8} rad in a very short computational time—this corresponds to a distance of about 80 km in the orbital motion.

For the first three cases, the values of Δv_{CR3BP} appear very similar to Δv_{Case3} ; however, for asteroid 2016RD34, the difference is considerable. We conjecture that this has to do with the close proximity to the Hill radius of this solution, as we can see on Figure 9b. As such, for this specific case, we have allowed for a relaxation of the targeting error up to 10^{-3} rad (about four times the previous distance) in order to check similar solutions. The obtained Δv_{CR3BP} becomes 90 m/s, a fact that reiterates the increased sensitivity of the motion around Hill sphere and the need for cohesive establishment of the limits in which adequate solutions can be found, something that has been brought to attention by Sánchez et al.⁷

On Table 2, it is possible to see the categories these asteroids fall into, the target LPO and the times of flight of the capture trajectory with and without the resonant encounter. It is obvious that the savings in fuel cost are contrasted by the increased time of flight taken by the capture; since we are considering one extra synodic period, the trajectory takes roughly twice as long.

5 Conclusions and Future Work

The trajectories analysed show great promise in reducing Δv costs of capturing asteroids into LPO. This is relevant in terms of mission design, since fuel consumption is one of the primary impactors of the cost of a space mission, and as such one of the main constraints limiting their boldness. However, the savings in fuel cost have to be weighted against the increased time of flight spent in the entire capture. This is a matter of trade-off analysis that can be performed for a specific mission design. Furthermore, a careful selection of the synodic period of the capture, by itself, is also valuable for cost reduction.

In summary, we have presented a new tool, supported by a dynamical model of motion of low computational cost, that proves to be very efficient in the design of optimal resonant encounters. This tool can be applied to the study of several interesting cost-saving trajectories in other planetary configurations and missions, such as Jovian moon tours.

The KM is shown to behave very similarly to the CR3BP and to adequately model the complexity of low energy resonant motion in asteroids where there is no transition and its distance to the Earth is always greater than Hill radius. Further work should consider the analysis of the boundaries of the KM, meaning the exact limits where it stops being a good approximation to a higher fidelity model.

In regards to resonant capture trajectories, further work will focus on the entire optimization of the manoeuvres, without resorting to the filter described in Section 3.0.1; instead of admitting a bi-impulsive manoeuvre estimate, an optimized Lambert arc will be considered. Furthermore, the use of low-thrust systems in the computation of these trajectories will also be studied and compared to current chemical thrust solutions.

References

1. Gómez G, Koon WS, Lo MW, Marsden JE, Masdemont J, Ross SD (2004) Connecting Orbits and Invariant Manifolds in the Spatial Restricted Three-Body Problem. *Nonlinearity* 17(5)
2. Koon WS, Lo MW, Marsden JE, Ross SD (2000) Heteroclinic Connections Between Periodic Orbits and Resonance Transitions in Celestial Mechanics. *Chaos: An Interdisciplinary Journal of Nonlinear Science* 10:427–469
3. Park P, Chamberlin A (2017) Horizons JPL Asteroid Database. <http://ssd.jpl.nasa.gov/horizons.cgi#top> Accessed: 2017-01-10
4. Ross SD, Scheeres DJ (2007) Multiple Gravity Assists, Capture, and Escape in the Restricted Three-Body Problem. *SIAM Journal on Applied Dynamical Systems* 6:576–596
5. Rudenko M (2017) Minor Planet Center Asteroid Database. <http://www.minorplanetcenter.net/iau/TheIndex.html>. Accessed: 2017-01-10
6. Sánchez JP, Alessi EM, Yárnoz DG, McInnes C (2013) Earth Resonant Gravity Assists for Asteroid Retrieval Missions. 64th International Astronautical Congress 2013 13
7. Sánchez JP, Colombo C, Alessi EM (2015) Semi-Analytical Perturbative Approaches to Third Body Resonant Trajectories. *Proceedings of the International Astronautical Congress, IAC* 7:5504–5515
8. Sánchez JP, Yárnoz DG (2016) Asteroid Retrieval Missions Enabled by Invariant Manifold Dynamics. *Acta Astronautica*
9. Strange N, Landau D, Lantoine G, Lam T, McGuire M, Burke L, Martini M, Dankanich J (2013) Overview of Mission Design for NASA Asteroid Redirect Robotic Mission Concept. 33rd International Electric Propulsion Conference
10. Szebehely V (1969) *Theory of Orbit*. Academic Press
11. Yárnoz DG, Sánchez JP, McInnes CR (2013) Easily Retrievable Objects Among the NEO Population. *Celestial Mechanics and Dynamical Astronomy* 116:367–388

Optimization of asteroid capture missions using Earth resonant encounters

Neves, Rita

2018-02-11

Attribution-NonCommercial 4.0 International

Rita Neves, and Joan Pau Sánchez. Optimization of asteroid capture missions using Earth resonant encounters. In: Vasile M., Minisci E., Summerer L., McGinty P. (eds) Stardust Final Conference on Asteroids and Space Debris, Volume 52, 2018

https://doi.org/10.1007/978-3-319-69956-1_1

Downloaded from CERES Research Repository, Cranfield University